AIAA SciTech Forum
8–12 January 2018, Kissimmee, Florida
2018 AIAA/ASCE/AHS/ASC Structures, Structural Dynamics, and Materials Conference

10.2514/6.2018-1442

Design of a wing tip device for active maneuver and gust load alleviation

Federico Fonte* Francesco Toffol† Sergio Ricci ‡
Department of Aerospace Science and Technology
Politecnico di Milano, 20156 Milano, Italy

In the present work the design of a wing tip device is presented along with the definition of the maneuver load controller and the gust load controller. A parametric sensitivity study has been performed to define the aerodynamic shape of the device, considering its effect on the dynamic properties of the aeroelastic system. After defining the aerodynamic shape the maneuver load alleviation controller and the gust load alleviation controller are described, the former is obtained by finding the distribution of surface deflections that can minimize the internal loads in a trim condition, while for the latter two different strategies are compared, one based on a static output feedback controller and the second based on a recurrent neural network controller. The active wing tip extension designed results able to contribute to the alleviation of wing dynamic loads and can compensate the increment of such loads resulting from the span extension.

I. Introduction

Most of the applications of active controllers for gust and maneuver load alleviation are based on the use of the standard control surfaces of the aircraft, usually ailerons and elevator. There are however some exceptions where the controllers had the possibility to use dedicated control surfaces for load alleviation. One particular situation where additional control surfaces are used occurs when fuselage modes need to be controlled, as in the case of the LAMS system[1] or the fuselage mode suppression system mounted on the B-1 Lancer aircraft.[2] There are also examples of aircraft equipped with control surfaces dedicated to gust alleviation, like the GLAS surface mounted on the B-2[3] and the Direct Lift Control (DLC) flaps mounted on the ATTAS aircraft.[4] Dedicated control surfaces were also studied in wind tunnel models, in[5] a trailing edge surface was used for load alleviation but resulted not very effective, different configurations of wing tip surfaces were applied to the EuRAM model[6] and a series of numerical studies[7,8] provide an example of the good performances of the devices. A canard was used in the wind tunnel test described in[9] complementing the use of a split aileron, while a set of four trailing edge flaps and a leading edge surface were used on the sensorcraft wing in,[10] with the purpose of giving to the controller the possibility to alleviate the gust without affecting the capability to manoeuvre the aircraft.

A particular configuration that can be used for providing an aircraft with additional control surfaces for load alleviation consists in designing a wing tip equipped with an actively controlled surface. Increasing the span of an aircraft has the advantage of improving its aerodynamic efficiency, but usually at the expense of an increase in loads. The increase in loads can be avoided by designing the chord and twist distribution of the wing in order to obtain a desired value of wing root bending moment,[11,12] but in many applications the wing tip extension need to be applied as a retrofit for an existing aircraft, in that case it is not possible to redesign the wing to limit the load increase. For this configurations Withcomb showed that winglets are more suitable than wing tip for increasing the aerodynamic efficiency,[13] an optimization study performed

*PhD Candidate, Department of Aerospace Science and Technology, Politecnico di Milano, Via La Masa 34, 20156 Milano, Italy, federico.fonte@polimi.it.
†PhD Candidate, Department of Aerospace Science and Technology, Politecnico di Milano, Via La Masa 34, 20156 Milano, Italy, francesco.toffol@polimi.it.
‡Full Professor, Department of Aerospace Science and Technology, Politecnico di Milano, Via La Masa 34, 20156 Milano, Italy, sergio.ricci@polimi.it.

in,[14] however, further analysed the differences between winglets and wing tip and showed how the optimal solution can depend on the maximum lift coefficient required, with the winglet performing better when manoeuvring conditions with high lift coefficients are included in the analysis.

One way to overcome the limitations in the performances of the wing tip extensions is to provide some active or passive alleviation capability, for example in[15] a wing tip extension for an A300 aircraft was designed, using aeroelastic tailoring for passive manoeuvre load alleviation and coupling it with an active gust load alleviation system. Other examples of wing tip designed for passive load alleviation can be found in,[16] where two concepts of a rigid wing tip with elastic attachment and an optimised composite wing tip were analysed. Similar analysis were performed in a series of studies performed within the ALPES project to a concept of folding wing tip, optimising the hinge line direction along with the attachment stiffness and damping.[17–19] The passive design can be complemented with the design of active components installed in the wing tip, for example in the Clean Sky project a wing tip equipped with a morphing leading edge was designed, with its shape defined using a parametric analysis,[20–22] leading to a predicted fuel weight savings of 2% and with a location of the elastic axis designed for allowing some load alleviation. Finally, a series of recent studies focused on the design of a winglet with an active trailing edge used for gust load alleviation.[23,24]

In the present work a wing tip extension equipped with a movable control surface is designed for an already existing reference aircraft. The reference aircraft is a model of a regional turboprop aircraft, shown in Fig. 1a. The selected configuration follows the same structure as the one presented in[24] consisting in a wing tip extension equipped with a trailing edge control surface, as shown in Fig. 1b. The dimensions and the geometry of the wing tip extension are selected to maximise the alleviation capabilities of the device.

Placing a control surface at the wing tip has some disadvantages from the point of view of the load alleviation, one limitation is in the small surface available, both due to the wing taper and to limitations in the increase in span. The chord and span of the wing tip need indeed to be limited taking in account also limitation not directly related to the gust load alleviation problem, for example the cost of airport gates that depends on the aircraft span.

A second limitation related to the wing tip configuration is the small distance from the added control surface and the elastic axis of the wing, this distance could be exploited to increase the effectiveness of the controller, as done in.[8] The aircraft considered in the present study, however, has a very high torsional stiffness of the wing, this can reduce the potential benefits coming from the use of an aerodynamic surface placed far from the elastic axis.

A third limitation is related to the position of the control surface close to the wing tip, where there is a strong effect of the wing tip vortices and the aerodynamic loads are the lowest in the wing. On the other hand also the hinge moments required for the actuation will be lower, partially compensating this disadvantage.

In addition to the above mentioned limitations related to the use of an active wing tip for load alleviation there are also advantages related to this configuration, the first one is the possibility to combine the load alleviation capability with an increase of aerodynamic efficiency coming from the span extension. In the limit the increase in efficiency could be seen as the main goal of the wing tip design, with the gust load alleviation system used to compensate the increase in wing loads coming from the extension, as actually done with the L-1011 aircraft[25] and in the theoretical studies on the A300 aircraft.[15] Another advantage obtained from the wing tip configuration is the availability of more room to host the actuation system with respect to the configurations studied in,[8] where the active surfaces were placed in front of the wing.

The main purpose of the active wing tip extension is to alleviate dynamic gust loads, this will be obtained through the implementation of a feedback control law based on the measurement of accelerations on several points on the aircraft structure. The results obtained with the active wing tip will be compared with the results that can be obtained by simply equipping the baseline aircraft with a gust alleviation system. Two different control systems are designed for the baseline aircraft, a Static Output Feedback controller[26] and an adaptive Recurrent Neural Network controller.[27]

The active wing tip can also be used for maneuver loads alleviation, that is to modify the lift distribution on the aircraft during maneuvers in order to reduce structural loads.[28] Maneuver load alleviation controllers can be designed when the number of available control surfaces is higher than the minimum required for the equilibrium of the aircraft, and two different approaches can be followed for its design. The first approach consists in the definition of a dynamic controller for maneuver load alleviation[29,30] while the second one is based on a static analysis of the maneuver conditions. In this way an optimal distribution of surface deflections is defined for each condition, leading to the formulation of pre-selected gains relating the measurements

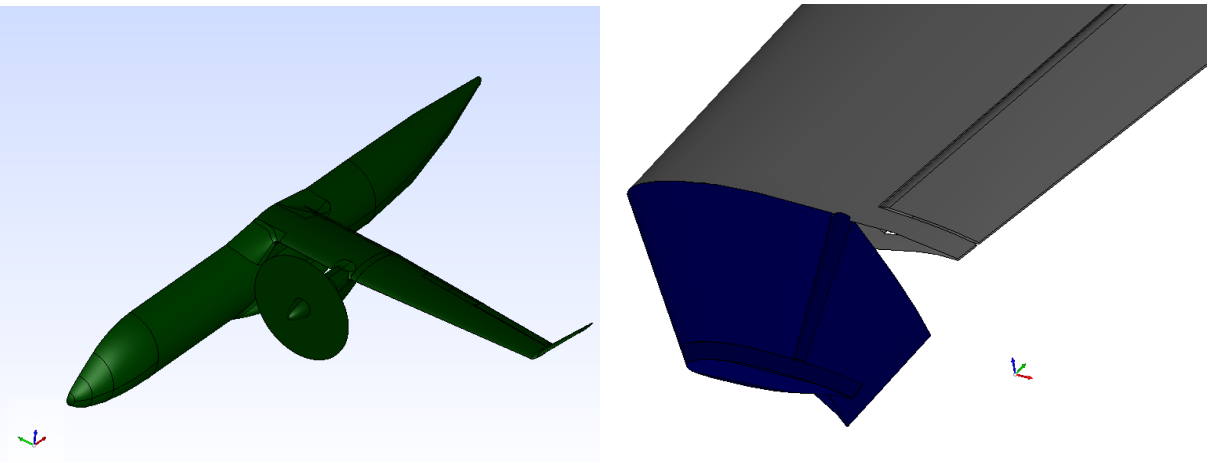

(a) Regional turboprop aircraft used as baseline configuration.

(b) Concept of the wing tip with trailing edge control surface.

Figure 1: Baseline model and active wing tip.

of the aircraft rigid state with the control surface deflection command. This latter approach will be followed in this work, formulating the trim solution as an optimization problem and computing the control surface deflection able to minimize the wing root bending moment.

II. Reference aircraft

The reference aircraft represents a generic turboprop transport aircraft, with a t-tail configuration and high wing. The reference model is already equipped with winglets, as shown in Fig. 1a, that are removed for allowing the installation of the wing tip device. The aeroelastic numerical model is composed by a beam model for the definition of the structure and by a lifting surface model for the computation of aerodynamic forces, as shown in Fig. 2. The aeroelastic analyses on the model were performed using SMARTCAD, the aeroelastic analysis module of the NeoCASS suite.[31] The aircraft resulted free from flutter throughout all the flight envelope, in particular the bending and the torsional modes of the wing are well decoupled thanks to the high torsional stiffness of the wing that leads to a ration of 9.119 between the frequencies of the torsional and bending natural modes.

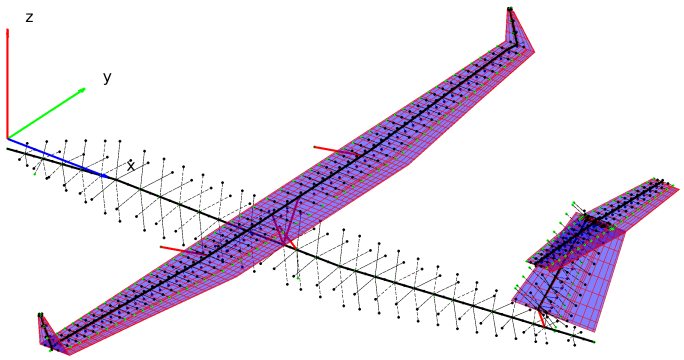

Figure 2: NeoCASS Aeroelastic model of the reference aircraft.

The SMARTCAD module is used for the frequency-domain analyses of the aircraft and also for the

generation of the time-domain state-space model of the aeroelastic system, used for the design of the control laws. The algorithm described in[32] is used for the generation of the time domain unsteady aerodynamic forces, while the approach already described in[33] is used for expressing the equations in body axes instead of in inertial coordinates.

III. Design of the wing tip device

The sizing of the wing tip is performed by first parametrizing its geometry and then analysing the effect of the rotation of the wing tip surface on the wing loads. The parameters used for the definition of the geometry are listed in Table 1 and represented in Fig. 3, they allow the definition of the planform with parameters like the span and the sweep angle, in addition also the dihedral angle can be modified allowing the modification of the configuration from a pure wing tip to a winglet. An additional non-geometric parameter is introduced, consisting in the possibility to switch between a traditional configuration with a trailing edge control surface and a configuration with an all-movable wing tip.

Name	symbol
Inboard chord ratio	$\frac{c_1}{c_{tip}}$
Taper ratio	$\frac{c_2}{c_1}$
Flap hinge location	$\frac{e}{c_1}$
Sweep angle	λ
Span	L
Dihedral angle	δ
Flapped vs. all movable	–

Table 1: Parameters defining the geometry of the wing tip.

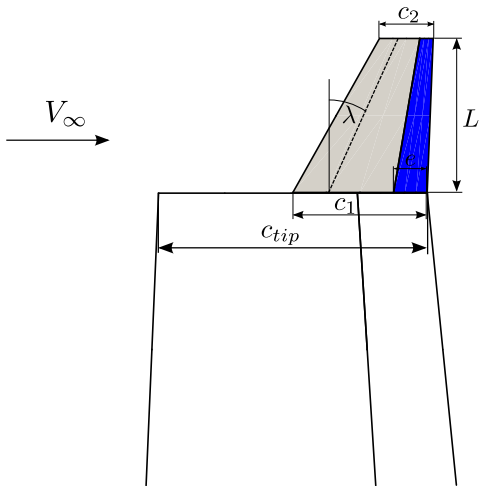

Figure 3: Schematic view of the wing tip

All the possible wing tip configuration needed to be compared considering the influence of the wing tip on wing loads, the norm of the transfer function between the control surface deflection and the loads is used to obtain a numerical measure of this influence, with the transfer function defined as

$$z = H(j\omega)\delta_{wt} \tag{1}$$

The variable z in Eq. (1) represents the desired performances and is composed by the wing root bending

moment, the wing root torsional moment and the hinge moment on the wing tip surface. δ_{wt} is the deflection of the wing tip control surface. The use of the frequency domain transfer function for the comparison of the configurations has the advantage of avoiding the need for the generation of the state-space model of the aerodynamic system, that would have been difficult to automatize for the application to the parametric study. In addition the open loop transfer function is used, then the results are not affected by the particular design of the control laws giving a more direct comparison of the configurations.

Among the cost index considered the most important is the transfer function from the wing tip deflection and the wing root bending moment H^{WRBM}. This index provides an indication on how much the wing tip is able to affect the resulting moment at wing root, and represent an upper limit for the alleviation capabilities of the gust load alleviation control system. Another important index is the transfer function between the surface deflection and surface hinge moment, which is directly related to the power required for the gust alleviation.

Two different measures of the transfer function considered: the steady response $H(0)$ and the quadratic norm restricted to a given frequency interval,

$$\|H(j\omega)\|_2 = \left[\int_{\omega_1}^{\omega_2} |H(j\omega)|^2 d\omega\right]^{\frac{1}{2}} \tag{2}$$

The frequency interval have the zero frequency as the lower limit, and a frequency of 10 Hz as upper limit, chosen in order to represent the limitation in bandwidth of the actuator system.

After some preliminary analyses the inboard chord ratio to has been fixed to an unit value, in order to maximize the surface of the wing tip and at the same time avoid sharp variation in chord along the span of the aircraft, potentially leading to the generation of aerodynamic vortexes.

Another parameter removed from the set of the ones considered in the analyses is the selection between the flapped and the all-movable configuration, selecting a standard flapped configuration. The performances of the all-movable device were strongly affected by the location of the hinge line, with the possibility to place the hinge line in a neutral position where no torque need to be applied to rotate wing tip. The neutral position is critical for the flutter point of view, while configurations with the hinge line downstream with respect to the neutral position can lead to divergence problems, thus requiring a minimum amount of actuator stiffness, and the necessary redundancy for ensuring the reliability of the system. The configurations with the hinge line upstream with respect to the neutral position, on the other hand, require large actuation torque compared with the flapped configuration, without providing a substantial increment in the alleviation capability.

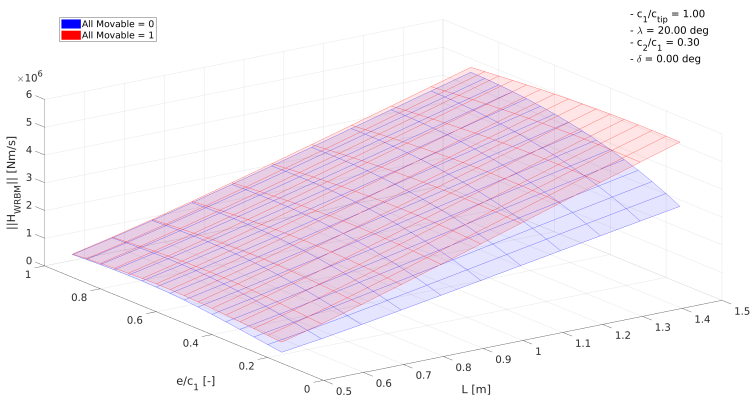

Figure 4: Response surface, norm of the transfer function from surface deflection to wing root hinge moment

One example of the results of the parametric analyses is presented in Fig. 4, where the response surface of the transfer function between the wing tip control surface deflection and the wing root bending moment is presented, considering its norm. The surface is obtained by evaluating the system for several values of the wing tip span and by varying the fraction of the wing tip chord dedicated to the control surface, both the all-movable and the flapped configurations are presented. It can be noticed that the variation of the norm

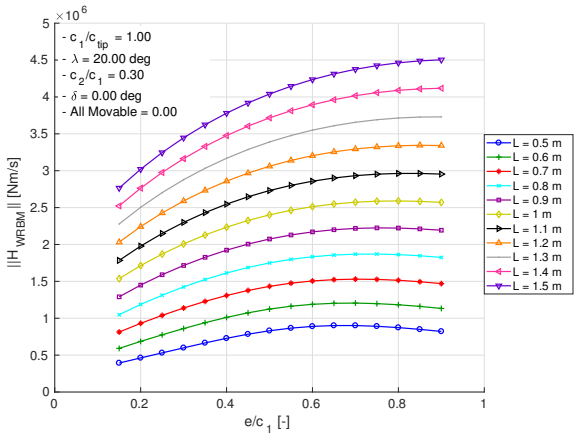

(a) Wing root bending moment

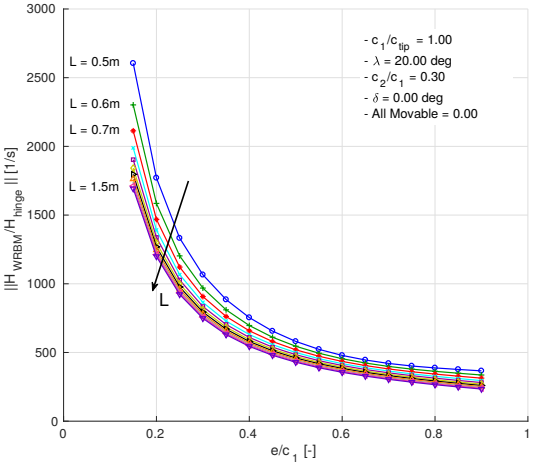

(b) Ratio wing root bending over surface hinge moment

Figure 5: Variation of the wing root bending moment and of the hinge moment with the control surface fraction e/c_1

with the increase in span is almost linear, both for the flapped and for the all-movable configurations, the effect of the increase of the surface chord fraction, instead, is not linear and it assumes different meaning and effects for the two configurations. For the flapped configuration the increase in surface chord has the expected effect of increasing the effectiveness of the surface, for the all-movable configuration, instead, the ratio e/c_1 represents the chord-wise position of the hinge line, and from Fig. 4 it can be seen that a more backward position of the hinge line increases slightly the effect of the surface on the wing root bending moment.

The variation of the effect on the wing toot bending moment of the surface chord fraction is presented also in Fig. 5a, for the flapped configuration only. It can be seen that the curves obtained for lower values of the wing tip span presents lower variations and have a maximum point for values of e/c_1 less than one. The position of the maximum changes with L and it is outside the considered range of values of e/c_1 for L higher than 1.3 m. By considering the effect on the wing root bending moment only, then, the limit on the surface chord ratio would be imposed from external constraints, like the structural sizing and the availability of space for the installation of the actuation system, but a limit on the value of e/c_1 can come also from the analysis of the dynamic response if the ratio between the wing root bending moment and the hinge moment is considered. This ratio is presented in Fig. 5b, and shows how the ratio increases with the decrease of the surface chord, meaning that the hinge moment decrease faster than the wing root bending moment. Since the bending moment over hinge moment ratio can be interpreted as a measure of the efficiency of the device it is desired to avoid low values for this quantity, the choice of the surface ratio must then be given by a trade-off between a good efficiency and a good effectiveness, and a value of $e/c_1 = 0.35$ is selected in this case.

The effects of a variation of the taper ration and of the sweep angle are presented in Fig. 6. The bending moment to hinge moment ratio for different values of the taper ratio is presented in Fig. 6a, showing that the most efficient configurations are the ones with a smaller ratio, which are also the less effective. Here an intermediate configuration with taper ratio $c_2/c_1 = 0.5$ was chosen.

The effect of the sweep is shown in Fig. 6b, showing that the configurations with the highest value of the bending to hinge moment ratio are those with negative sweep angle. In this case, however, a configuration with positive sweep was preferred, and values of λ close to zero were discarded because, in combination with the selected taper ratio, led to a sharp variation of the trailing edge line, with a negative sweep of the trailing edge line. A configuration with $\lambda = 35°$ was then selected, in order to be beyond the minimum of Fig. 6b. In this way a racked wingtip with a backward swept trailing edge is obtained, that can lead to a reduction of induced drag.[34]

A complete analysis of the wing tip requires also the evaluation of the effect of the configuration change

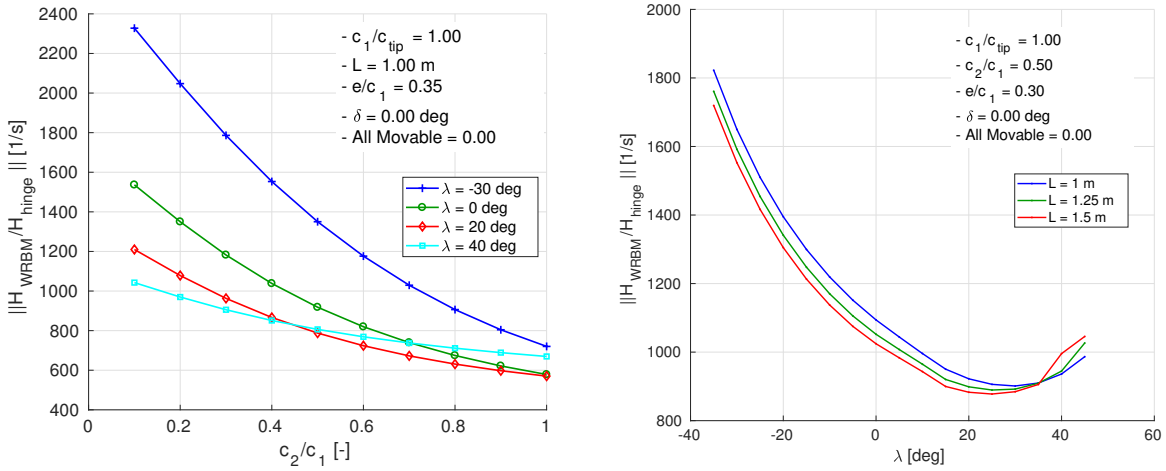

(a) Variation of taper ratio.

(b) Variation of sweep angle.

Figure 6: Ratio wing root bending over surface hinge moment for different taper ratios and sweep angles

in the open loop gust loads. Following the same approach used for evaluating the effect of the wing tip surface deflection the transfer function from the gust angle α_g and the loads in the wing is defined

$$z = G(j\omega)\alpha_g \tag{3}$$

in particular it results that an increase in wing span lead to an increase of gust loads, thus reducing the overall effectiveness of the wing tip control surface. The load increase can be reduced by introducing some dihedral angle, with the effect of keeping unchanged the surface of the wing tip, but reducing the net area affected by vertical gusts.

The effect of the dihedral angle can be seen in Fig. 7, where a configuration with a wing tip span $L = 1.5$ m is analysed. The three curves in the plot represent the norm of the transfer functions $H(j\omega)$ and $G(j\omega)$ for different values of the dihedral angle. The transfer function $H(j\omega)$ represents the maximum reduction achievable using a wing tip device, two different curves for $H(j\omega)$ are plotted representing the standard flapped configuration and the all-movable configuration. A reference configuration was chosen in order to have the same dihedral angle as the winglet of the baseline model, $\delta = 85°$, the gust transfer function $G(j\omega)$ presented in Fig. 7 represents the increment with respect to this reference configuration and was obtained by subtracting the value of $G(j\omega)$ obtained with $\delta = 85°$ from all the other values.

It can be seen that the effect of the surface grows faster than that of the gust by reducing the dihedral angle, thus for the configurations with moderate to high dihedral angle the net effect of the introduction of the control surface is maximum, with a sharp decrease around 25° of dihedral where there is a large increase in gust load accompanied by small variations in the control surface effectiveness. The same behaviour can be observed for both the configuration with standard flapped surface and the one with all-movable device, but with an increase in maximum alleviation in the latter case. The all-movable configuration corresponding to this plot, however, had a rearward hinge line position that would have required a minimum amount of actuator stiffness to avoid divergence problems.

$\frac{c_1}{c_{tip}}$	$\frac{c_2}{c_1}$	$\frac{e}{c_1}$	λ	L	δ
1	0.5	0.35	35°	1 m	0°

Table 2: Parameters defining the selected configuration.

The selected configuration is characterized by a standard flapped surface and the parameters presented in Table 2. Based on the considerations on the gust load sensitivity one possible configuration can be characterized by a moderate dihedral angle, as shown in Fig. 8a, where a span 1.5 m is used. Another

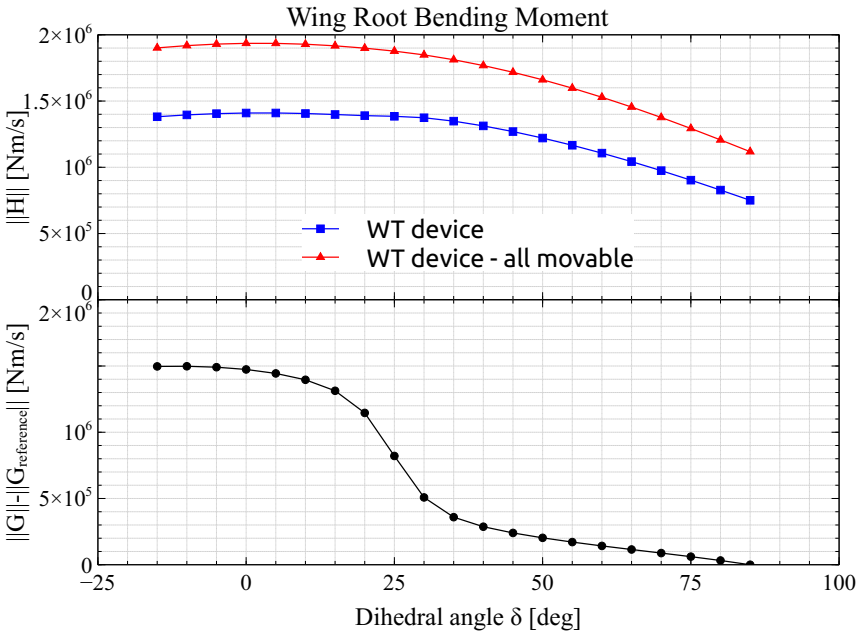

Figure 7: Comparison between the effect of the gust and that of the wing tip control surface on wing root bending moment, using a reference configuration with dihedral angle $\delta = 85°$, span $L = 1.5$ m.

possibility to avoid a large increase in open loop gust loads is based on the use of a shorter span as shown in Fig. 8b. This represents a compromise solution since the capability of the control surface is limited with respect to the case with dihedral angle, but it has the advantage of leading to a smaller span, leading also to a lower weight increase.

IV. Structural Design

A structural model of the wing tip was developed based on the selected geometric configuration. The model, shown in Fig. 9, has the aim of evaluating the mass and stiffness properties of the device, as well as allowing the design of the actuation system. A conventional aluminum wing box is designed using C-shaped spars, and four stiffeners (two for each side) with T cross section; the movable part is linked to the wingtip box by two hinges placed on the inner and outer ribs.

The sizing of the surface is performed considering maneuver and dynamic gust loads on the open loop model. The load conditions are defined according to the CS-25 regulations,[35] introducing also some load conditions associated with the maximum deflection of the wing tip control surface (limited to 15°).

The distribution of the Von Mises stress on the structure is presented in Fig. 10. The maximum Von Mises stress has a value of $\sigma_{VM\ max} = 150$ MPA, below the yield limit of 500 MPa associated to the Al7075-T6 aluminum considered, although the rotation of the wing tip control surface is considered among the sizing maneuver conditions, the maximum Von Mises loads occurs with a symmetric 2.8 g pull-up and a roll maneuver that give the maximum loads for the skin and the spar caps respectively. The same load conditions together with the torque required by the controller are used to draw the load envelope for the actuation system.[36]

V. Maneuver Load Alleviation

A static maneuver load controller can be designed exploiting the availability of redundant control surfaces with respect to the ones required by the equilibrium of the aircraft. The controller can be then designed in a static way, as a set of gains that are computed and then associated to each maneuver condition.

Since more control surfaces are available than the ones required for the trim and maneuver conditions it

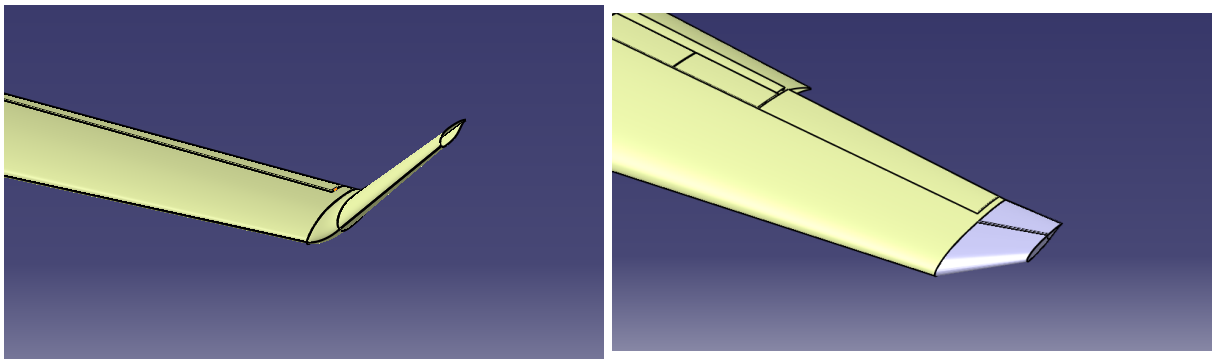

(a) Configuration with dihedral angle

(b) Configuration with no dihedral

Figure 8: Selected configurations for the wing tip device

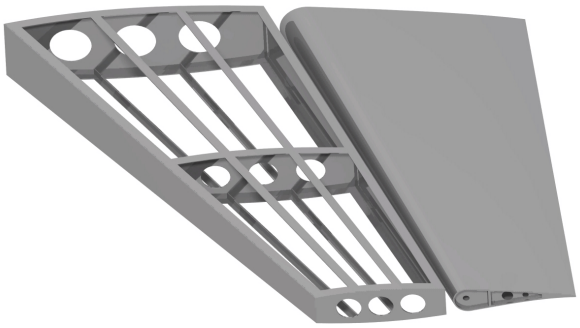

Figure 9: Structural layout of the wingtip

is then possible to solve the aeroelastic trim problem and at the same time minimize a cost function related to some quantity of interest, for example the internal loads at the wing root. The cost function will be in general a quadratic function of the generalized displacement vector $\boldsymbol{q}$, the control surface deflection $\boldsymbol{u}_c$ and the external load $\boldsymbol{\mathcal{F}}_g$

$$J(\boldsymbol{u}_c) = \frac{1}{2}\begin{bmatrix}\boldsymbol{q}^T & \boldsymbol{u}_c^T & \boldsymbol{\mathcal{F}}_g^T\end{bmatrix}\begin{bmatrix}\boldsymbol{S}_{qq} & \boldsymbol{S}_{qc} & \boldsymbol{S}_{qf}\\ \boldsymbol{S}_{cq} & \boldsymbol{S}_{cc} & \boldsymbol{S}_{cf}\\ \boldsymbol{S}_{fq} & \boldsymbol{S}_{fc} & \boldsymbol{S}_{ff}\end{bmatrix}\begin{bmatrix}\boldsymbol{q}\\ \boldsymbol{u}_c\\ \boldsymbol{\mathcal{F}}_g\end{bmatrix} \tag{4}$$

The static aeroelastic problem is formulated for the modally reduced system as

$$\begin{aligned}\bar{\boldsymbol{\mathcal{K}}}(q_\infty, M)\boldsymbol{q} + \bar{\boldsymbol{\mathcal{K}}}_c(q_\infty, M)\boldsymbol{u}_c &= \boldsymbol{\mathcal{F}}_g(N_z)\\ \boldsymbol{N}\boldsymbol{q} &= \bar{\boldsymbol{q}}\end{aligned} \tag{5}$$

where $\boldsymbol{\mathcal{F}}_g(n_z) = \boldsymbol{U}^T\boldsymbol{f}_g$ is the vector with the generalized inertia forces, computed from the complete vector of inertia forces $\boldsymbol{f}_g$. The matrix $\bar{\boldsymbol{\mathcal{K}}}(q_\infty, M)$ contains both the structural and aerodynamic stiffness and is a function of the dynamic pressure and Mach number. The second equation represents a set of linear constraints used to define the trim condition in terms of the flight condition, for example by imposing the sideslip angle or the pitch rate.

From the solution of Eq. (5) it is possible to extract the stresses or the internal forces in the structure by means of a summation of forces method

$$\boldsymbol{\sigma} = \boldsymbol{S}_\sigma\left(\boldsymbol{f}_g + q_\infty \boldsymbol{K}^a(M)\boldsymbol{U}\boldsymbol{q} + \bar{\boldsymbol{K}}_c(q_\infty, M)\boldsymbol{u}_c\right) \tag{6}$$

where $\boldsymbol{S}_\sigma$ is a matrix relating the nodal displacements to the internal forces and stresses. Instead of solving

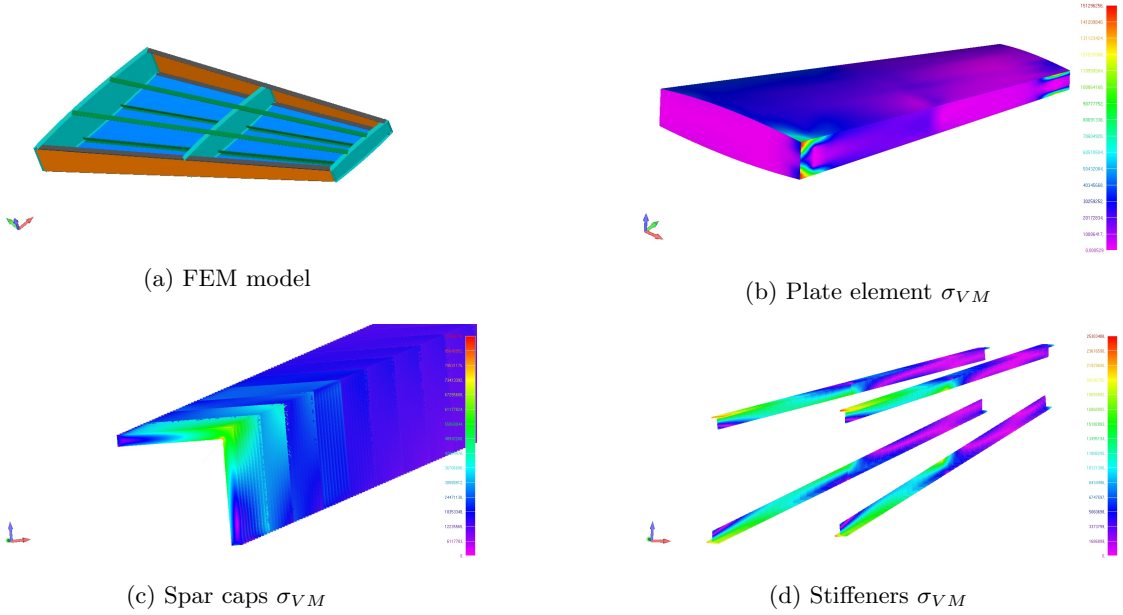

(a) FEM model

(b) Plate element σ_{VM}

(c) Spar caps σ_{VM}

(d) Stiffeners σ_{VM}

Figure 10: Structural model of the wing tip device and stress analysis results

Eq. (5) directly the following constrained minimization problem is solved

$$\begin{aligned} &\min_{\boldsymbol{u}_c} J(\boldsymbol{u}_c) \\ &\text{subject to} \\ &\quad \bar{\boldsymbol{\mathcal{K}}}(q_\infty, M)\boldsymbol{q} + \bar{\boldsymbol{\mathcal{K}}}_c(q_\infty, M)\boldsymbol{u}_c = \boldsymbol{\mathcal{F}}_g(N_z) \\ &\quad \boldsymbol{N}\boldsymbol{q} = \bar{\boldsymbol{q}} \end{aligned} \tag{7}$$

The problem in Eq. (7) can be solved by using the Lagrange multiplier method, leading to the solution of the following linear system

$$\begin{bmatrix} \boldsymbol{S}_{qq} & \boldsymbol{S}_{qc} & \bar{\boldsymbol{\mathcal{K}}}(q_\infty, M)^T & \boldsymbol{N}^T \\ \boldsymbol{S}_{cq} & \boldsymbol{S}_{cc} & \bar{\boldsymbol{\mathcal{K}}}_c(q_\infty, M)^T & \boldsymbol{0} \\ \bar{\boldsymbol{\mathcal{K}}}(q_\infty, M) & \bar{\boldsymbol{\mathcal{K}}}_c(q_\infty, M) & \boldsymbol{0} & \boldsymbol{0} \\ \boldsymbol{N} & \boldsymbol{0} & \boldsymbol{0} & \boldsymbol{0} \end{bmatrix} \begin{bmatrix} \boldsymbol{q} \\ \boldsymbol{u}_c \\ \boldsymbol{\lambda} \\ \boldsymbol{\Phi} \end{bmatrix} = \begin{bmatrix} -\boldsymbol{S}_{qf}\boldsymbol{\mathcal{F}}_g \\ -\boldsymbol{S}_{cf}\boldsymbol{\mathcal{F}}_g \\ \boldsymbol{\mathcal{F}}_g \\ \bar{\boldsymbol{q}} \end{bmatrix} \tag{8}$$

A constraint in the amplitude of the deflection of the control surface should be introduced in the optimization problem, but in order to obtain an analytical solution a different approach is followed here, that is the amplitude of the control surface deflection is controlled by including it in the cost function. This approach is completely analogous to that used in the definition of the cost function of the LQR controller.

In order to show the capabilities of this approach the method is applied to compute the surface deflections required for a trim condition with load factor $N_z = 2.5$. The computed deflections are presented in Table 3, showing that the use of multiple surfaces is able to reduce the maneuver bending moment by 7.8%, leading also to an increase of trim angle of attack of almost 0.5°. The internal load distribution along the wing span is shown in Fig. 11, for the shear force, the torsional moment and the bending moment. It can be seen that the decrease in bending moment is obtained through concentrating the lift, and then the shear force, toward the inboard section of the wing. At the same time there is an increase in torsional moment, needed to counteract the hinge moment of the aileron and the wing tip device surface. By allowing the use of more control surfaces, like flaps and spoilers it would be possible to find a better compromise between the reduction in bending moment and torsional moment.

	Direct trim solution	LAC approach
Angle of attack	8.064°	8.672°
Elevator deflection	−8.237°	−8.651°
Aileron deflection	0°	−4.524°
deflection WT device	0°	−7.265°
Wing root bending moment	1.914×10^6 Nm	1.764×10^6 Nm

Table 3: Deflections and angle of attack with the single- and multiple-surface approaches

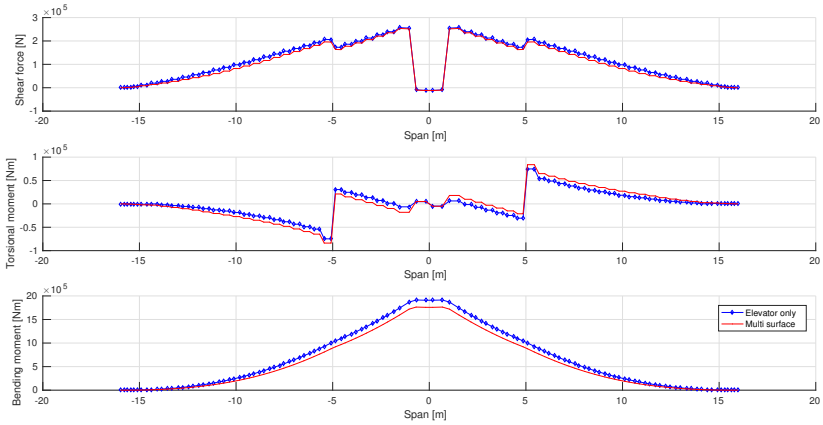

Figure 11: Spanwise load distribution using a single or multiple surfaces.

VI. Gust Load Alleviation Controllers

Two different control strategies are applied to the design of the gust load alleviation controller on the baseline aircraft. The first strategy consists in the use of a static output feedback controller, designed on the analytic model of the aircraft. The second approach consists in the use of a neural network controller whose parameters are trained online without any need for the numerical model of the aircraft.

All the presented simulations are performed considering a model of the control surface actuation system with 15 Hz bandwidth, and saturations both in maximum deflection angle and in the maximum deflection rate.

A. Static Output Feedback Controller

The Static Output Feedback (SOF)[26] is based on the use of an algebraic relationship between the measurements $\boldsymbol{y} \in \mathbb{R}^{l_y}$ extracted from the system and the control input $\boldsymbol{u} \in \mathbb{R}^{m_u}$, defined by a gain matrix $\boldsymbol{G}$ such that $\boldsymbol{u} = \boldsymbol{G}\boldsymbol{y}$. The gain matrix is computed by the minimization of the $\mathcal{H}_2$ norm of the closed loop transfer function, relating some external disturbance to the performance output $\boldsymbol{z}$, which can be expressed as a function of the gain matrix as

$$J(\boldsymbol{G}) = \frac{1}{2}\int_0^\infty [\mathbf{z}^\mathbf{T}\mathbf{W}_{\mathbf{zz}}\mathbf{z} + \mathbf{u}^\mathbf{T}\mathbf{W}_{\mathbf{uu}}\mathbf{u}] \tag{9}$$

$\mathbf{W}_{\mathbf{zz}}$ and $\mathbf{W}_{\mathbf{uu}}$ are weighting matrices that are used to define the relative importance of the components of the control input and of the performance output. In the present work the algorithm presented in[37] is used for the minimization of the cost function $J(\boldsymbol{G})$.

The controller is based on the use of accelerometric measurements taken on the wing, as well as the rigid motion of the aircraft obtained from an Inertial Measurement Unit (IMU), the location of the sensors is shown in Fig. 12. The torsional and bending moments are the main targets of the GLA controller, the pitch

angle and rate are included in the cost function with a small weight in order to ensure an adequate damping for the rigid motion of the aircraft. The evaluation of the closed loop transfer function requires also the definition of the disturbances, which are taken to be the gust input and the noise on the measurements, with a shaping filter used to define the frequency content of the gust in order to reproduce that of a deterministic 1-cos gust.

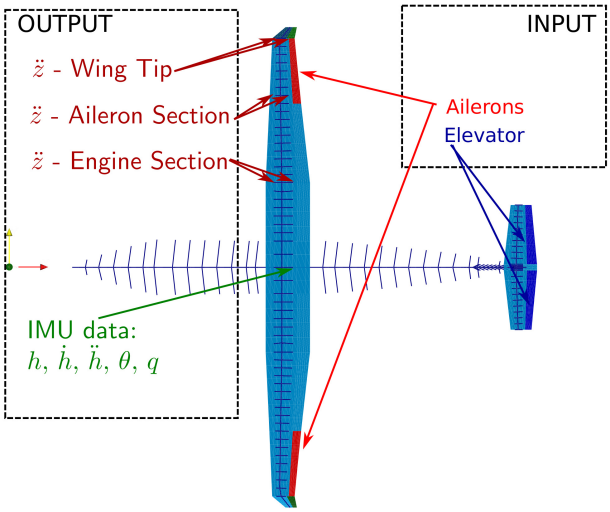

Figure 12: Configuration of the SOF controller for the baseline model.

In Fig. 13 and 14 the results of the application of the controller on the gust response analysis are presented, considering a sea level flight condition with a deterministic $1 - cos$ gust with frequency $f_g = 0.705 f_{bend}$, where f_{bend} is the natural frequency of the first wing bending mode of the aircraft.

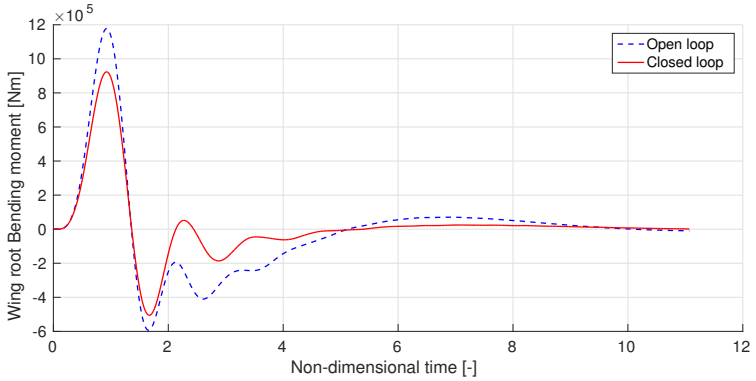

Figure 13: SOF control: Time history of wing root bending moment.

B. Neural Network Controller

The second control strategy uses a Recurrent Neural Network controller[33,27] which is based on the use of two different neural networks: the first one is used as an identifier, and provides an one-step-ahead prediction of the system output. The second one is a control network, it uses the predicted output generated by the first network and computes the control input needed to drive the output to a desired value. An overview of the controller is presented in Fig. 15.

The weights of the network are trained on-line, using a gradient descent method based on the minimization of the reconstruction error for the identification network and the minimization of the tracking error for the control network.

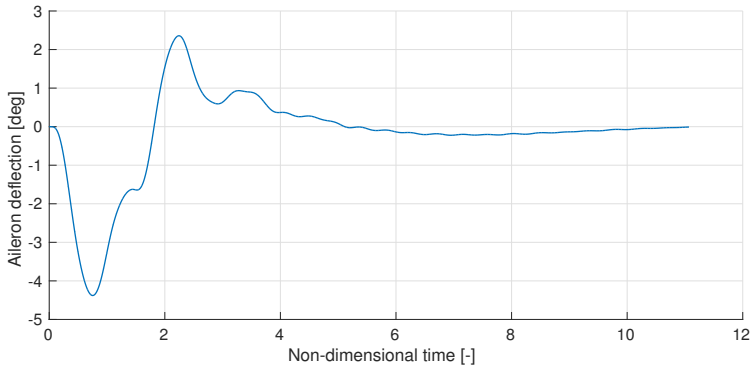

Figure 14: SOF control: Aileron deflection.

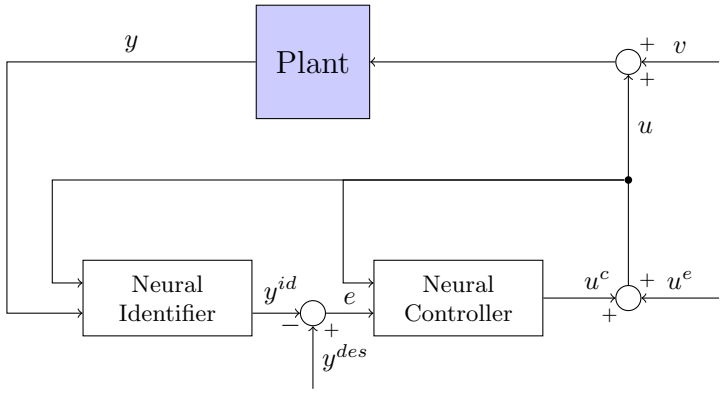

Figure 15: Scheme of the RNN controller

The controller is implemented considering the vertical acceleration at the center of mass of the aircraft as measurement, while the symmetric deflection of the ailerons is used as control input.

In Fig. 16b and Fig. 16a are presented the results obtained by applying the network to the aircraft numerical model on a steady level flight at sea level, and computing the response to a 1-cos gust with frequency $f_g = 0.705 f_{bend}$. The results are shown only for the case when the only actuated surface is the aileron, and show that a reduction of the wing root bending moment of about 22% is can be obtained with a surface deflection of about 6°. From the aileron time history in Fig. 16a it is possible to notice the effect of the actuator transfer function in the definition of the actual control surface deflection.

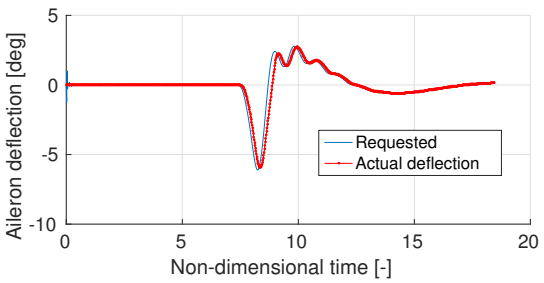

(a) Aileron deflection.

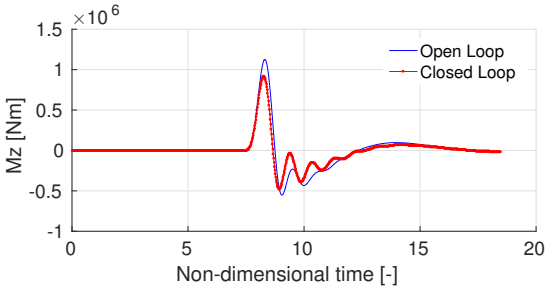

(b) Wing root bending moment.

Figure 16: Closed loop response to gust using the RNN controller

VII. GLA control using wingtip

The results presented above form the basis for the comparison of the performances of the wing tip device, in particular the results obtained with the static output feedback controller will be extended to the case with the active wing tip installed. The design procedure used for the definition of the SOF controller is replicable and the same cost function can be applied to different models, in this way there is a more direct correlation between the closed loop results obtained with the different configurations with respect to the neural controllers, whose performances depends both on the configuration and on the training procedure. This is the reason on the basis of the choice of the SOF controller for the comparison of the closed loop results obtained with the active wing tip, instead of the recurrent neural network controller.

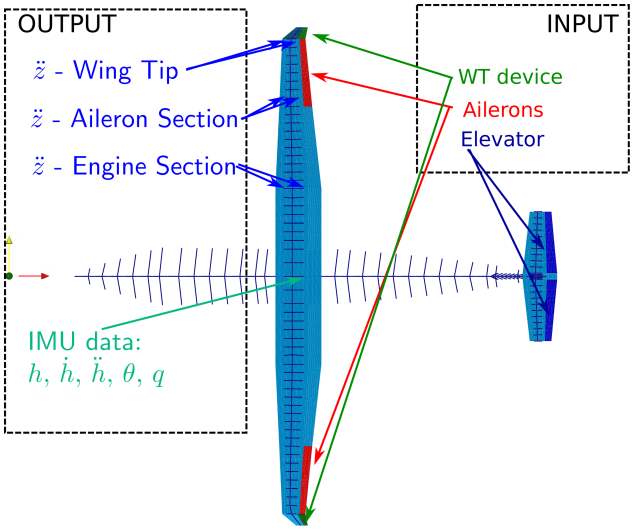

Figure 17: Configuration of the SOF controller for the model with active wing tip.

The basic configuration used for the definition of the controller is presented in Fig. 17, the configuration is identical to the one used for the baseline controller and shown in Fig. 12, with the addition of the wing tip control surface. Also the cost function used for the optimization of the gain matrix is unchanged. The wing tip surface is included among the control input with a lower weight with respect to aileron and elevator reflecting the fact that while aileron and elevator are primary control surfaces used to maneuvering the aircraft, the wing tip surface can be devoted completely to gust load alleviation.

The wing root bending moment and the control surfaces deflection histories are shown in Fig. 18, showing the alleviation possible with a deflection of about 4° of the aileron, similar to the deflection used in the baseline model, and with about 10° of wing tip surface deflection.

It is interesting also to check the capabilities of the wing tip control surface alone in alleviating gust loads, and in Fig. 19, showing a reduced alleviation with respect to the one obtained using also ailerons, but still able to compensate the incremental load introduced by the span extension. This can be seen also in Fig. 20, where the distribution of bending moment along wing span is displayed. It can be seen that both wing tip configurations provide an increment in wing root bending moment with respect to the baseline aircraft, but in both cases the movement of the wing tip surface only is able to recover this increment, with a larger gain in the case of wing tip with dihedral angle.

VIII. Conclusions and Future Work

The activity presented in this paper is aimed at the evaluation of the capabilities of an active wing tip device designed for maneuver and gust load alleviation. The design is performed by means of a parametric sensitivity analysis, based on the dynamic properties of the system. Further refinement of the shape of the device can be obtained by considering also the aerodynamic efficiency, even if this is not the primary goal of the device. The presence of redundant control surfaces allowed the definition of the trim problem as a constrained optimization problem, allowing the reduction of wing internal load, and the analyses performed

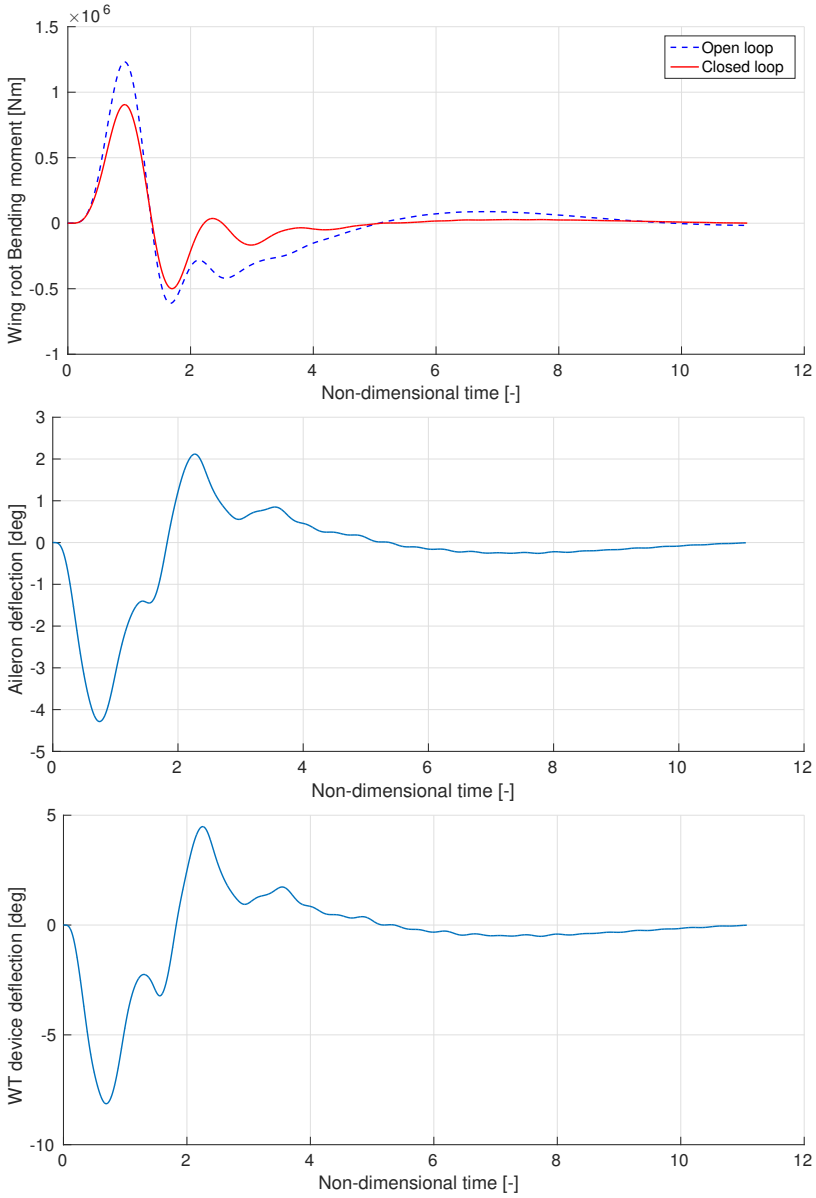

Figure 18: Gust response ZFW sea level, $f_g = 0.705 f_{bend}$. SOF control for the wingtip without dihedral angle

showed that an explicit solution of the optimization problem is possible, without the need of the introduction of constraints in the control surfaces deflections. This static load alleviation capability is combined with a dynamic gust and turbulence load controller in order to provide an overall reduction of the load envelope on the wing. Two different control strategies for the gust load alleviation controller were implemented, a Static Output Feedback (SOF) controller based on the numerical model of the system and a Recurrent Neural Network controller, designed without any need for a numerical model of the aircraft. The two controllers are evaluated on the reference aircraft and showed similar alleviation capabilities. The SOF controller was also used to compare the loads obtained with the baseline model with those obtained using the active wing tip. The results shows how the use of the active wing tip can improve the performances of the controller by providing some additional alleviation capability with respect to the movement of the aileron. An increase in span is associated with an increase of the aerodynamic efficiency of the wing, for this reason it is often desired to increment the aspect ratio of an existing aircraft but this lead inevitably to an increase in dynamic gust loads. The device presented in this work is able to completely compensate the increment in gust loads,

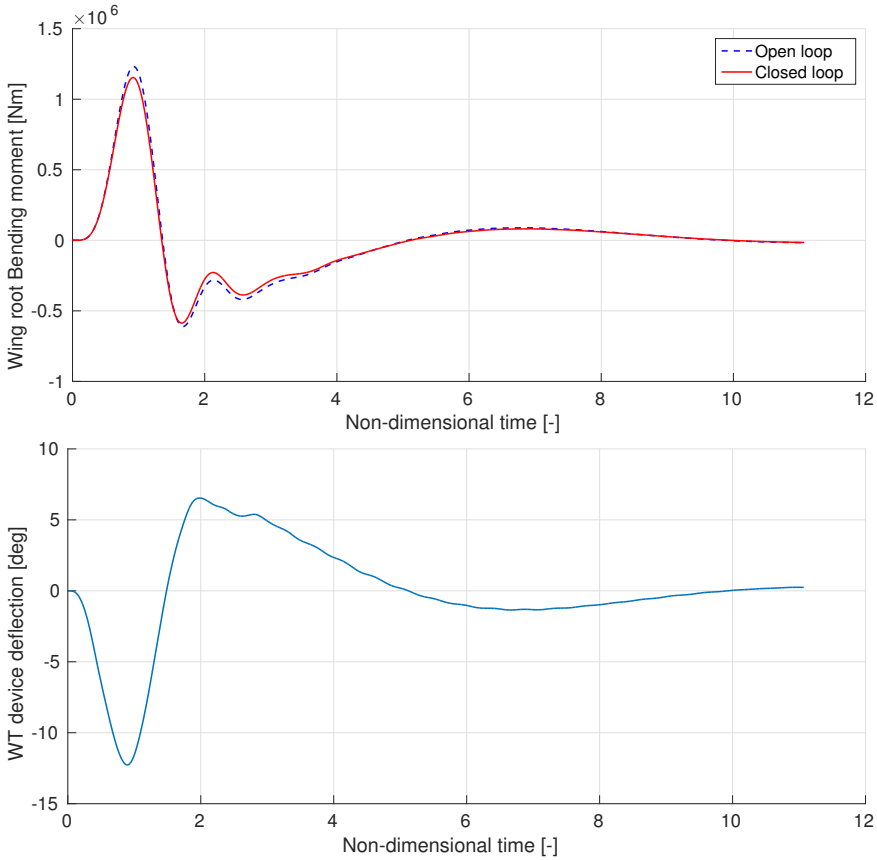

Figure 19: Gust response ZFW sea level, $f_g = 0.705 f_{bend}$. SOF control for the wingtip without dihedral angle, using only the WT surface.

thus the active wing tip extension can be seen as a technique to increase the wing span without affecting the wing internal loads.

IX. Acknowledgment

The research leading to these results has received funding from the European Communitys Seventh Framework Programme (FP7/2007-2013) for the Clean Sky Joint Technology Initiative under grant agreement CSJU-GAM-GRA-2008-001 and the European Communitys Horizon 2020 - the Framework Programme for Research and Innovation (2014-2020) for the Clean Sky Joint Technology Initiative under grant agreement CS2-REG-GAM-2014-2015-01.

References

[1]Burris, P. M. and Bender, M. A., "Aircraft Load Alleviation and Mode Stabilization (LAMS): B-52 System Analysis, Synthesis, and Design," Tech. rep., Air Force Flight Dynamics Laboratory. Air Force Systems Command. Wright-Patterson Air Force Base, Ohio, 1969.

[2]Regan, C. D. and Jutte, C. V., "Survey of Applications of Active Control Technology for Gust Alleviation and New Challenges for Lighter-weight Aircraft," Tech. rep., NASA, TM–2012-216008, 2012.

[3]Britt, R. T., Volk, J. A., Dreim, D. R., and Applewhite, K. A., "Aeroservoelastic Characteristics of the B-2 Bomber and Implications for Future Large Aircraft," Tech. rep., DTIC Document, 2000.

[4]Hahn, K.-U. and Schwarz, C., "Alleviation of atmospheric flow disturbance effects on aircraft response," *26th Congress of the International Council of the Aeronautical Sciences (ICAS), Anchorage, Alaska, USA (September 2008)*, 2008.

[5]Matsuzaki, Y., Ueda, T., Miyazawa, T., and Matsushita, H., "Wind tunnel test and analysis on gust load alleviation of a transport-type wing," *87-0781. 28th Structures, Structural Dynamics and Materials Conference*, 1987.

[6]Kuzmina, S. I., Ishmuratov, F., Zichenkov, M., and Chedrik, V., "Integrated numerical and experimental investigations

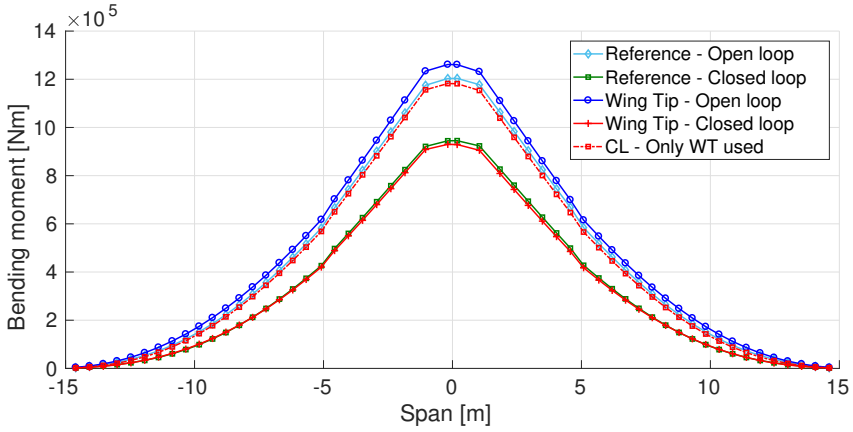

(a) No dihedral

Figure 20: Bending moment distribution along wing span. ZFW sea level, $f_g = 0.705 f_{bend}$.

of the Active/Passive Aeroelastic concepts on the European Research Aeroelastic Model (EuRAM)," *Journal of Aeroelasticity and Structural Dynamics*, Vol. 2, No. 2, 2011, pp. 31–51.

[7]Karpel, M., Moulin, B., Feldgum, V., et al., "Active alleviation of gust loads using special control surfaces," *47th AIAA/ASME/ASCE/AHS/ASC Structures, Structural Dynamics, and Materials Conference, 1-4 May 2006, Newport, Rhode Island*, Vol. AIAA 2006-1833, 2006.

[8]Moulin, B. and Karpel, M., "Gust loads alleviation using special control surfaces," *Journal of Aircraft*, Vol. 44, No. 1, 2007, pp. 17–25.

[9]Wu, Z., Chen, L., and Yang, C., "Study on gust alleviation control and wind tunnel test," *Science China Technological Sciences*, Vol. 56, No. 3, 2013, pp. 762–771.

[10]Vartio, E., Shimko, A., Tilmann, C. P., and Flick, P. M., "Structural modal control and gust load alleviation for a sensorcraft concept," *Proceedings of the 46th AIAA/ASME/ASCE/AHS/ASC Structures, Structural Dynamics & Materials Conference, Austin, TX, USA*, 2005, pp. 18–21.

[11]Tollmien, W., Schlichting, H., Görtler, H., and Riegels, F., "Über Tragflügel kleinsten induzierten Widerstandes," *Ludwig Prandtl Gesammelte Abhandlungen*, Springer, 1961, pp. 556–561.

[12]Jones, R. T., "The spanwise distribution of lift for minimum induced drag of wings having a given lift and a given bending moment," Tech. rep., NACA, Tn–2249, 1950.

[13]Whitcomb, R. T., "A design approach and selected wind tunnel results at high subsonic speeds for wing-tip mounted winglets," Tech. rep., NASA, TN D-8260, 1976.

[14]Ning, A. and Kroo, I., "Multidisciplinary considerations in the design of wings and wing tip devices," *Journal of Aircraft*, Vol. 47, No. 2, 2010, pp. 534–543.

[15]Sensburg, O., Becker, J., Lusebrink, H., and Weiss, F., "Gust Load Alleviation on Airbus A 300," *ICAS-82-2.1.1*, 1982.

[16]Ricci, S., Castellani, M., and Romanelli, G., "Multi-fidelity design of aeroelastic wing tip devices," *Proceedings of the Institution of Mechanical Engineers, Part G: Journal of Aerospace Engineering*, Vol. 227, No. 10, 2013, pp. 1596–1607.

[17]Castrichini, A., Siddaramaiah, V. H., Calderon, D., Cooper, J. E., Wilson, T., and Lemmens, Y., "Nonlinear Folding Wing Tips for Gust Loads Alleviation," *Journal of Aircraft*, Vol. 53, No. 5, 2016, pp. 1391–1399.

[18]Castrichini, A., Cooper, J. E., Wilson, T., Carrella, A., and Lemmens, Y., "Nonlinear Negative Stiffness Wingtip Spring Device for Gust Loads Alleviation," *Journal of Aircraft*, Vol. 54, No. 2, 2017, pp. 627–641.

[19]Cheung, R., Castrichini, A., Rezgui, D., Cooper, J., and Wilson, T., "Testing of Wing-Tip Spring Device for Gust Loads Alleviation," *58th AIAA/ASCE/AHS/ASC Structures, Structural Dynamics, and Materials Conference. 9 - 13 January 2017, Grapevine, Texas*, Vol. 1317, 2014.

[20]Chekkal, I., Cheung, R., Wales, C., Cooper, J. E., Allen, N., Lawson, S., Peace, A. J., Hancock, S., Cook, R., Standen, P., and Carossa, G. M., "Design of a morphing wing tip," *Proceedings of the AIAA SciTech 22nd AIAA/ASME/AHS Adaptive Structures Conference, National Harbor, MD, USA*, Vol. 1317, 2014.

[21]Cooper, J. E., Chekkal, I., Cheung, R. C. M., Wales, C., Allen, N. J., Lawson, S., Peace, A. J., Cook, R., Standen, P., Hancock, S. D., and Carossa, G. M., "Design of a Morphing Wingtip," *Journal of Aircraft*, Vol. 52, No. 5, Jul 2015, pp. 1394–1403.

[22]Vasista, S., Riemenschneider, J., Van de Kamp, B., Monner, H. P., Cheung, R. C., Wales, C., and Cooper, J. E., "Evaluation of a Compliant Droop-Nose Morphing Wing Tip via Experimental Tests," *Journal of Aircraft*, Vol. 54, No. 2, 2016, pp. 519–534.

[23]Heinen, C., Wildschek, A., and Herring, M., "Design of a winglet control device for active load alleviation," *International forum on aeroelasticity and structural dynamics, Bristol, UK*, 2013, pp. 24–26.

[24]Wildschek, A., Prananta, B., Kanakis, T., Tongeren, H., and Huls, R., "Concurrent optimization of a feed-forward gust loads controller and minimization of wing box structural mass on an aircraft with active winglets," *16th AIAA/ISSMO multidisciplinary analysis and optimization conference, Dallas, TX*, 2015, pp. 22–26.

[25]Johnston, J. F., "Accelerated development and flight evaluation of active controls concepts for subsonic transport aircraft. Volume 1: Load alleviation/extended span development and flight tests," Tech. rep., NASA-CR-159097, September 1979.

[26]Syrmos, V. L., Abdallah, C. T., Dorato, P., and Grigoriadis, K., "Static Output Feedback — A Survey," *Automatica*, Vol. 33, No. 2, 1997, pp. 125–137.

[27]Bernelli-Zazzera, F., Mantegazza, P., Mazzoni, G., and Rendina, M., "Active Flutter Suppression Using Recurrent Neural Networks," *Journal of Guidance, Control, and Dynamics*, Vol. 23, No. 6, 2000, pp. 1030–1036.

[28]Thornton, S. V., "Reduction of structural loads using maneuver load control on the Advanced Fighter Technology Integration (AFTI)/F-111 mission adaptive wing," Tech. rep., NASA, TM-4526, 1993.

[29]Giesseler, H.-G. and Beuck, G., "Design procedure for an active load alleviation system (LAS) for a modern transport aircraft," *Congress of the International Council of the Aeronautical Sciences (ICAS), Toulouse, Fr (1984)*, 1984.

[30]Company, B. C. A., "Integrated Application of Active Control (IAAC) Technology to an advanced subsonic transport project — Final Act Configuration Evaluation," Tech. rep., NASA, CR–3545, 1982.

[31]Cavagna, L., Ricci, S., and Travaglini, L., "NeoCASS: An integrated Tool for Structural Sizing, Aeroelastic Analysis and MDO at Conceptual Design Level," *Progress in Aerospace Sciences*, Vol. 47, 2011, pp. 621–635.

[32]Ripepi, M. and Mantegazza, P., "Improved Matrix Fraction Approximation of Aerodynamic Transfer Matrices," *AIAA Journal*, Vol. 51, No. 5, 2013, pp. 1156–1173.

[33]Fonte, F. and Mantegazza, P., "A Recurrent Neural Network Controller for Gust Load Alleviation on a Transport Aircraft," *58th AIAA/ASCE/AHS/ASC Structures, Structural Dynamics, and Materials Conference. Grapevine, Texas.*, 2017.

[34]Kroo, I. and Smith, S., "The computation of induced drag with nonplanar and deformed wakes," *SAE 901933, SAE Transactions*, 1990.

[35]AAVV, "Certification Specifications for Large Aeroplanes CS-25," amendment 7 ed., European Aviation Safety Agency, October 2009, Annex to ED Decision 2009/013/R.

[36]Toffol, F., Fonte, F., and Ricci, S., "Design of an Innovative Wing Tip Device," *International Forum on Aeroelasticity and Structural Dynamics, 25-28 June 2017, Como, Italy*, Vol. IFASD-198, 2017.

[37]Fonte, F., Ricci, S., and Mantegazza, P., "Gust load alleviation for a regional aircraft through a static output feedback," *Journal of Aircraft*, Vol. 52, No. 5, 2015, pp. 1559–1574.